Faraday Discussions

Cite this: *Faraday Discuss.*, 2017, **196**, 131

PAPER

Aggregation-induced enhanced green light emission from a simple donor–π–acceptor (D–π–A) material: a structure–property relationship study†

Vinod Kumar Gupta and Ram Adhar Singh*

Received 26th June 2016, Accepted 12th August 2016
DOI: 10.1039/c6fd00158k

Organic D–π–A materials, possessing intramolecular charge transfer, have attracted much scientific attention in recent years because of their potential applications in the development of organic light emitting devices (OLEDs). Two new compounds, **A1** and **A2**, having a D–π–A skeleton have been synthesized and single crystals were grown by the solution growth technique. Both compounds were characterized for crystallographic, thermal and photophysical properties. Upon photo-excitation in the solid state, **A1** showed very strong green light emission while **A2** gave sky-blue emission with much lower intensity. A single crystal X-ray diffraction study revealed that in the crystal lattice of **A1**, both the donor and acceptor groups are involved in the intermolecular interactions. This results in the restricted intramolecular rotation (RIR) of the D and A moieties, and enables **A1** to emit more intensely in the solid state due to aggregation-induced emission (AIE). Intense green light emission, along with a good crystalline nature indicates that **A1** might be a potential candidate for opto-electronic devices.

1. Introduction

Organic solid state light emitting materials offer great technological potential for developing optoelectronic devices such as OLED displays, optical data recording and storage media.[1–3] Efforts over the last two decades have resulted in a number of prototype devices based on these materials becoming commercially available.

Department of Chemistry, Centre of Advanced Study, Institute of Science, Banaras Hindu University, Varanasi-221 005, India. E-mail: prrasingh@gmail.com

† Electronic supplementary information (ESI) available: Copies of NMR and IR (^{1}H and ^{13}C) spectra for **A1** and **A2**. Details of single crystal growth. Crystallographic data in CIF format for **A1** and **A2**. Crystallographic parameters, list of bond lengths and bond angles. The UV-vis absorption spectra in different solvents. Fluorescence spectra in different solvents. Lippert–Mataga plots. Details of quantum yield calculation. DTA curve of **A1** and **A2**. Thermal activation energy plots. CCDC 1486589–1486590. For ESI and crystallographic data in CIF or other electronic format see DOI: 10.1039/c6fd00158k

However, the search for new and high performance stable materials goes on. In solid state fluorescence, intermolecular electronic interactions and molecular stacking modes play key roles.[4] Therefore, it is important to grow a single crystal of these materials to explore their crystallographic parameters for a better understanding of their light emitting behaviour in the solid state. Control of the molecular orientation and stacking modes of a fluorophore in the crystal lattice is an effective approach for tuning the luminescence properties of organic materials.[5] The emission induced by the restriction of intramolecular rotation (RIR) of fluorophores is termed aggregation-induced emission (AIE).[6,7] RIR blocks the non-radiative pathways and is the main origin of AIE.[8] AIE in organic systems was first discovered in a series of silole derivatives which were found to be non-emissive in solution but highly luminescent in the solid state.[6] Furthermore, AIE in organic donor–π–acceptor (D–π–A)[9,10] systems possessing intramolecular charge transfer (ICT) from the D end to the A end are of great interest due to their potential applications in two photon fluorescence and in the construction of OLEDs. Recently, Shen *et al.* have reported red to near infrared (NIR) solid state fluorescence in a fumaronitrile based fluorogen through AIE.[5] The existence of C–H$\cdots\pi$ interactions in the crystal lattice of the fluorogen restricts the intramolecular rotation of the D and A moieties, and enables the fluorogen to emit intensely in the solid state. These systems are bulky, involving multistep synthesis and are high cost. Also, single crystal growth of these materials is difficult due to quick nucleation, which leads to precipitation or the formation of poly-crystals. AIE has not yet been reported in a smaller D–π–A molecular system with easier synthesis and single crystal growth to fulfill the cost effectiveness requirements of opto-electronic devices.

In the present study, we report a comparative study of the solid-state light emitting behaviour of two simple organic D–π–A materials: 2-cyano-3-(2,4-dimethoxyphenyl)acrylamide (**A1**) and 2-cyano-3-(4-methoxyphenyl)acrylamide (**A2**) (Fig. 1). To the best of our knowledge no reports have been found related to the aggregation induced enhanced light emission effect in these compounds. However, **A1** has been recently reported as a potent inhibitor of tyrosinase and **A2** has been used as a precursor in organic synthesis.[11,12] Single crystal growth and crystallographic studies have been carried out on these compounds to determine the role of molecular packing in their solid state fluorescence. The thermal properties were investigated using differential scanning calorimetry (DSC) and

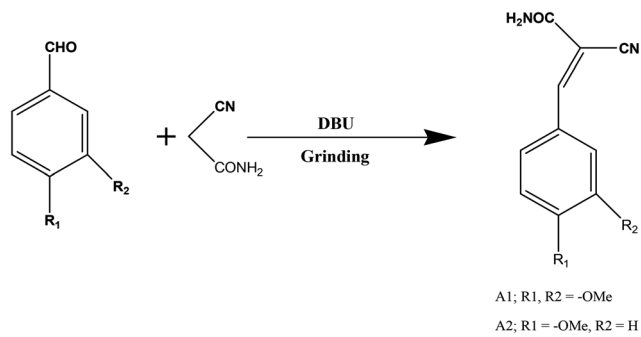

Fig. 1 Reaction scheme for the synthesis of A1 and A2.

thermogravimetric-differential thermal analysis (TG-DTA). UV-vis absorption and fluorescence spectra were recorded in different organic solvents with varying polarity and the quantum yields reported. Lippert–Mataga plots for both compounds were analysed and the change in dipole moment reported.

2. Experimental section

2.1. Materials and measurements

2,4-Dimethoxybenzaldehyde (Avra Chemical Pvt Ltd) was recrystallized from ethanol before use. Cyanoacetamide was purchased from Spectrochem Pvt Ltd and used as received. 1,8-Diazabicyclo[5.4.0]undec-7-ene (DBU) (Sigma Aldrich, USA) was also used as received. The solvents were distilled before use. All NMR spectra were recorded using a FTNMR-JEOL AL300 spectrometer using $CDCl_3$ as a solvent. X-ray diffraction data of single crystals were collected using the Xcalibur oxford CCD diffractometer. Structure solution and refinement were carried out using SHELXS and SHLEXL-97. DSC experiments were performed using a Mettler TA 4000 machine under a nitrogen atmosphere with a heating rate of 10 °C min^{-1}. However, thermogravimetric-differential thermal analysis (TG-DTA) was performed using a NETZSCH, STA 409 PC analyzer under a nitrogen atmosphere with a heating rate of 10 °C min^{-1} from room temperature to 500 °C. UV-vis absorption spectra were recorded using a Shimadzu UV-1700 model. Fluorescence spectra were obtained using a JY Horiba fluorescence spectrophotometer. All the spectra in solution have been recorded at 4 nm slit width and in the solid state at 2 nm slit width. The relative quantum yield has been calculated using anthracene as a reference compound.[13]

2.2. Synthesis of 2-cyano-3-(2,4-dimethoxyphenyl)acrylamide (A1)

Equimolar amounts of 2,4-dimethoxybenzaldehyde (1.66 g, 10 mmol) and 2-cyanoacetamide (0.84 g, 10 mmol) were mixed thoroughly, and then 1 mmol of DBU (0.15 g) was added. The reaction mixture was ground with a pestle and mortar for 60 seconds and then treated with cold water. A yellow solid was obtained. The product was filtered, dried and the crude compound was recrystallized from a mixture of acetone and methanol to obtain the desired compound in pure form. ^{1}H NMR (300 MHz, $CDCl_3$) δ (ppm): 8.74 (s, 1H, H–C=C–), 8.27 (d, 2H, Ar-H), 6.60 (d, 2H, Ar-H), 6.46 (s, 1H, Ar-H), 6.30 (br s, 2H, $-NH_2$), 5.83 (br s, 2H, $-NH_2$), 3.90 (s, 6H, $-CH_3$); ^{13}C NMR (75 MHz, $CDCl_3$) δ (ppm): 165.52, 162.97, 161.47, 147.91, 130.81, 130.81, 118.32, 105.99, 98.17, 55.70, 55.29; FT-IR (KBr) $\bar{\nu}$ (cm^{-1}): 3462.80, 3357.47, 2931.67, 2839.77, 2211.16, 1668.76, 1612.27, 1570.90, 1503.53, 1472.00, 1425.21, 1372.37, 1356.53, 1301.37, 1274.41, 1204.05, 1166.21, 1127.04, 1041.63, 1014.08, 802.04, 761.81, 661.05, 519.81 (Fig. S1, S2 and S5†).

2.3. Synthesis of 2-cyano-3-(4-methoxyphenyl)acrylamide (A2)

Equimolar amounts of 4-methoxybenzaldehyde (1.96 g, 10 mmol) and 2-cyanoacetamide (0.84 g, 10 mmol) were mixed thoroughly, and then 1 mmol of DBU (0.15 g) was added. The reaction mixture was ground with a pestle and mortar for 60 seconds and then treated with cold water. A white solid was obtained. The product was filtered, dried and the crude compound was recrystallized from a mixture of acetonitrile and acetone to obtain the desired compound in pure

form. ^{1}H NMR (300 MHz, $CDCl_3$) δ (ppm): 8.26 (s, 3H, H–C═C–), 7.96 (d, 2H, Ar-H), 6.99 (d, 2H, Ar-H), 6.27 (br s, 2H, –NH_2), 5.68 (br s, 2H, –NH_2), 3.89 (s, 3H, CH_3); ^{13}C NMR (75 MHz, $CDCl_3$) δ (ppm): 170.91, 153.44, 148.67, 146.96, 138.88, 135.80, 133.33, 114.78, 55.59; FT-IR (KBr) $\bar{\nu}$ (cm^{-1}): 3448.93, 3368.51, 3308.80, 3181.02, 2942.79, 2209.81, 1698.89, 1584.32, 1511.01, 1311.18, 1262.94, 1180.14, 1027.32, 828.14, 672.65, 580.18, 531.44 (Fig. S3, S4 and S6†).

3. Results and discussion

3.1. X-ray crystallographic studies

Single crystals of **A1** and **A2** were grown by slow evaporation of solvents (1 : 1 acetone–methanol and acetone–acetonitrile, respectively) at room temperature and analysed by X-ray crystallography. The crystal structure analysis gave the molecular structures of both compounds, which confirmed the proposed structures of the molecules. The crystal structures of **A1** and **A2** are shown in Fig. 2. Both crystals belong to the monoclinic system with space groups $P2_1/n$ and $P2_1/c$, respectively. The unit cell parameters for **A1** are $a = 10.5310(11)$ Å, $b = 15.6321(15)$ Å, $c = 13.7351(18)$ Å, and $\beta = 94.071(10)^\circ$; for **A2** $a = 3.9225(3)$ Å, $b = 10.7762(9)$ Å, $c = 23.142(2)$ Å, and $\beta = 93.453(7)^\circ$ (the crystallographic parameters for **A1** and **A2** are given in Table S1 and details of the bond angles and bond lengths are given in Table S2†).

The packing in space lattices of **A1** and **A2** are stabilized by various C–H···O and C–H···N molecular interactions. The crystal lattice of **A1** contains eight molecules per unit cell which are distributed in four parallel rows and each row contains two molecules (Fig. 3a). The molecules in **A1** are connected by C12–H12A···N1, N4–H4A···O2 and N4–H4B···O3 molecular interactions and form a layer. These layers are connected with each other by C11–H11A···N3 interaction and form a sheet structure (Fig. 4a). Apart from these interactions, the packing in **A1** is stabilized by intermolecular C–H···π interaction (Fig. 4c). In such an interaction, the phenyl ring of one molecule is connected to the vinyl-H of the other molecule. Two different centroid to vinyl-H distances were found; 3.53 and 3.84 Å. This provides some extra stability to the molecular packing. However, **A2** possesses four molecules per unit cell as shown in Fig. 3b. The molecules in the space lattice are connected by C3–H3···O2, N2–H2A···O1 and C11–H11A···N1 interactions. Apart from these interactions, there exists a C═O···HN– H-bond (2.06 Å) between two molecules. The distance between the π-electron density of the phenyl ring of one molecule and the aromatic-H/vinyl-H of the other molecule

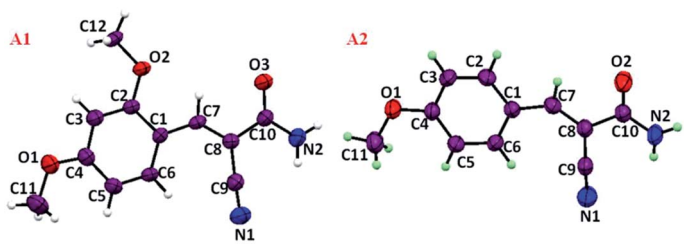

Fig. 2 The molecular structures of A1 and A2 showing displacement ellipsoids at the 50% probability level.

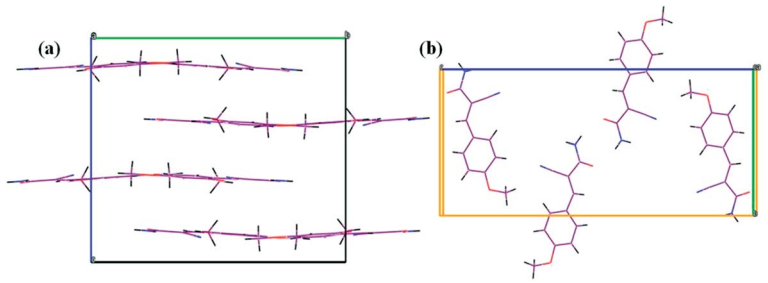

Fig. 3 Unit cell arrangement of molecules for (a) **A1** and (b) **A2**.

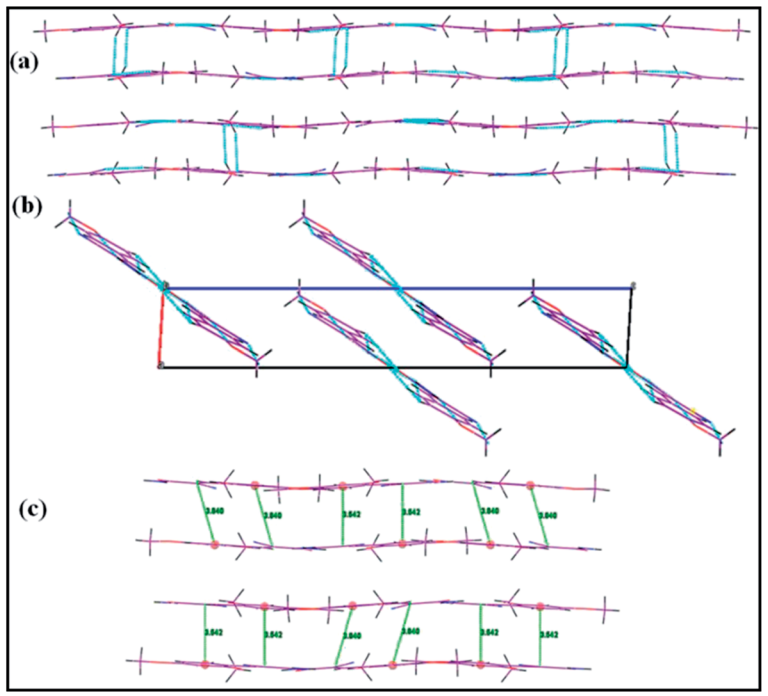

Fig. 4 (a) A view in projection down the *a*-axis of the crystal packing in **A1**, (b) a view in projection down the *b*-axis of the crystal packing in **A2** and (c) a representation of the C–H···π interactions in **A1**.

in **A2** is much higher (>11.0 Å). Therefore, no C–H···π interactions have been found in **A2**. A view in projection down the *b*-axis of the crystal packing in **A2** is represented in Fig. 4b. All the interactions for **A1** and **A2** are tabulated in Table 1.

3.2. Photophysical properties

The UV-vis absorption spectra of **A1** and **A2** in acetonitrile solution exhibit bands at 357 and 332 nm, respectively. These bands are characteristic of intramolecular charge transfer (ICT) π → π* transitions occurring from the donor (methoxy group/groups) to the acceptor cyano(aminocarbonyl)methylidene. The spectra are

Table 1 Short-contact geometry (Å, °) for A1 and A2

D–H···A	D–H	H···A	D···A	D–H···A
A1				
C11–H11A···N3	0.96	2.72	3.63	157.49
C12–H12A···N1	0.96	2.61	3.10	112.08
N4–H4A···O2	0.86	2.32	3.18	175.58
N4–H4B···O3	0.86	2.33	3.04	138.98
A2				
C3–H3···O2	0.96	2.59	3.36	140.59
N2–H2B···O2	0.86	2.06	2.91	168.51
N2–H2A···O1	0.86	2.58	3.39	142.86
C11–H11A···N1	0.96	2.70	3.51	142.52

shown in Fig. 5. The absorption spectrum of **A1** is slightly red-shifted (25 nm) which is due to the presence of one additional methoxy group at the *ortho* position with respect to the electron acceptor moiety. Therefore, dominating charge transfer from the donor to the acceptor in **A1** (through the +R effect) exists, and consequently a higher value of λ_{max} was obtained. The electronic absorption spectra were also recorded in various organic solvents with varying polarity (Fig. S7†). It has been found that the change of solvent polarity does not affect the λ_{max} value very much. The λ_{max} and molar extinction coefficient (ε) values in different solvents are listed in Table 2.

The solid state fluorescence spectra of **A1** and **A2** were recorded under similar conditions and are shown in Fig. 6a. Intense emission and pronounced red shift in the solid phase were found as compared with the solution phase, and this is

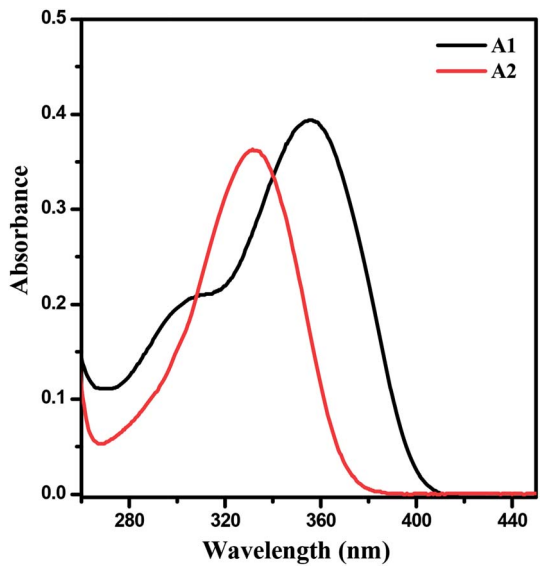

Fig. 5 Absorption spectra of A1 and A2 in acetonitrile with a molar concentration of 1.0×10^{-5} M.

Table 2 Optical properties of **A1** and **A2** in different solvents

Compound	Solvent	λ_{max}^{abs} (nm)	ε (L mol^{-1} cm^{-1})	λ_{max}^{emi} (nm)	$\Delta\bar{\nu}_{st}$ (cm^{-1})	Φ_F
A1	DMF	358	39 000	451	5760	0.0094
A1	MeCN	357	39 500	440	5284	0.0042
A1	MeOH	360	45 000	438	4947	0.0023
A1	Toluene	363	46 000	441	4820	0.0056
A2	DMF	332	33 000	410	5730	0.0058
A2	MeCN	332	36 000	408	5611	0.0097
A2	MeOH	334	36 000	412	5668	0.0038
A2	Toluene	337	37 000	411	5343	0.0110

attributed to the presence of interfluorophore interactions in the solid phase.[14,15] **A2** showed much stronger emission at 526 nm than **A1** (496 nm). This difference in the emission behaviour of **A1** and **A2** can be explained on the basis of their molecular packing in the lattice.

Restriction of intramolecular rotation (RIR) due to the existence of intermolecular interactions between the molecules rigidifies their molecular structures.[16] This process minimizes the non-radiative transitions and maximizes the possibility of radiative transitions. The emission induced by RIR is termed aggregation induced emission (AIE).[17,18] As discussed in the crystallographic studies (Section 3.1), in the crystal lattice of **A1** both the methoxy groups (donor end) and cyano(aminocarbonyl)methylidene group (acceptor end) are engaged in intermolecular interaction. Also, there exists a pronounced C–H$\cdots\pi$ interaction in **A1**. All of these interactions restrict the intramolecular rotation of the D and A moieties to a better extent than in **A2**, and enable **A1** molecules to emit more intensely in the solid state due to aggregation induced enhanced emission (AIEE). However, in the case of **A2** no C–H$\cdots\pi$ interactions exist. Therefore, it has comparatively lesser RIR and consequently a weaker intensity than **A1**. Under UV photo-excitation, **A1** shows intense green emission whereas **A2** shows sky-blue emission with much lower intensity than **A1**. The obtained visible color emission from **A1** and **A2** upon photo-excitation under a UV lamp is shown in Fig. 7.

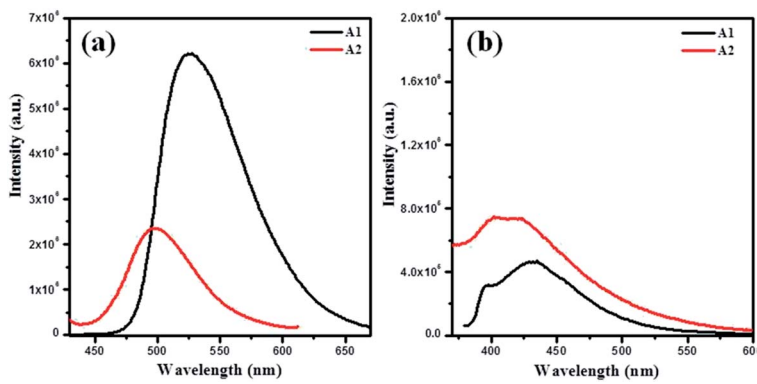

Fig. 6 Fluorescence spectra of **A1** and **A2** (a) in the solid state and (b) in acetonitrile with a molar concentration of 1.0 $\times$ 10^{-5} M at their λ_{max}(abs) excitations.

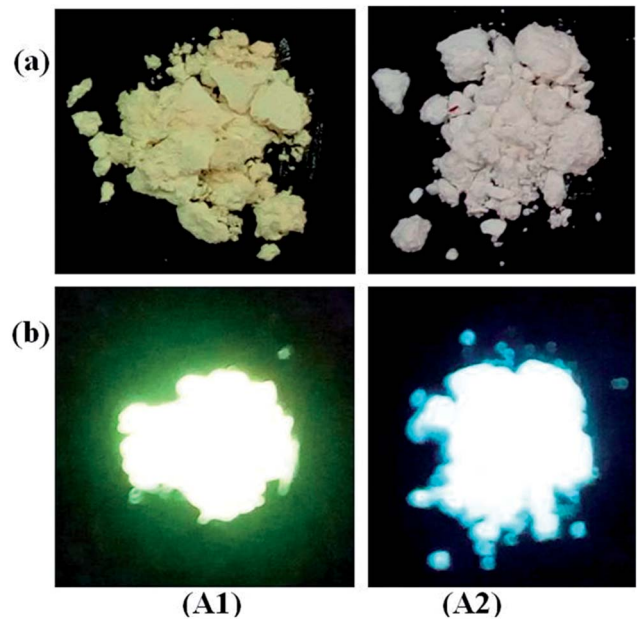

Fig. 7 Photographs showing color emission (a) under normal light and (b) under UV irradiation ($\lambda = 365$ nm) of **A1** and **A2** in the solid state.

In the solution phase both compounds showed poor fluorescence emission. The fluorescence spectra of compounds **A1** and **A2** in acetonitrile solution are shown in Fig. 6b. Compounds **A1** and **A2** exhibit emission bands at around 440 and 408 nm, respectively. The fluorescence spectra were also recorded in different organic solvents with varying polarity (Fig. S7†). As with the absorption spectra, the fluorescence behaviour is also not greatly affected by the nature of the solvent. Thus, we may conclude that the fluorescence properties of both the compounds are not very promising in solution, which is also clear from the lower quantum yields in different organic solvents.

The photo-excitation of an ICT material results in an increase in dipole moment due to an increase in polarity in the excited state. This change in dipole moment is directly related to the optical behaviour of the material, and its evaluation provides valuable information for the design of materials for various opto-electronic devices. The Lippert–Mataga equation for this evaluation is the most extensive and widely used method. This equation relates the Stokes shift to the dipole moment as shown in equation,[19,20]

$$\Delta\bar{\nu} = \bar{\nu}_{\max}^{\text{abs}} - \bar{\nu}_{\max}^{\text{emi}} = \frac{2(\mu_e - \mu_g)^2}{hca^3}\Delta f + \text{constant} \quad (1)$$

where $\Delta\mu = (\mu_e - \mu_g)$ is the change in dipole moment from the excited state (μ_e) to the ground state (μ_g), h = Planck's constant, c = velocity of light, and a = Onsager cavity radius, defined as $a = (3M/4\pi dN)^{1/3}$, where d is the density of the solute molecule, M is the molecular weight of the solute, N is Avogadro's number and Δf = Lippert–Mataga solvent polarity parameter, defined as:[21,22]

$$\Delta f = \left[\frac{(\varepsilon - 1)}{(2\varepsilon + 1)} - \frac{(n^2 - 1)}{(2n^2 + 1)}\right] \quad (2)$$

where ε is the static dielectric constant and n is the refractive index of the solvent. The plot of solvent polarity function *versus* Stokes shift results in a straight line (Fig. S8†), the slope of which gives the value of $\Delta\mu$. The values of $\Delta\mu$ for **A1** and **A2** are found to be 5.7 D and 5.6 D, respectively.

3.3. Thermal analysis

The thermal behaviour of **A1** and **A2** has been investigated with the help of TG-DTA and DSC studies. The TGA and DSC curves for **A1** and **A2** are shown in Fig. 8. The TGA curve shows that **A1** exhibits weight loss in two steps: 180–330 °C (52% weight loss) and 331–490 °C (13% weight loss) with about 35% char yield. **A2** also shows a similar two step decomposition pattern: 200–335 °C (61% weight loss) and 336–490 °C (17% weight loss) with about 22% char yield. The DTA curve (Fig. S9†) reflects one endothermic peak in the lower temperature region and one exothermic peak in the higher temperature region. The endothermic peak corresponds to the melting temperature of the compound and the exothermic peak corresponds to the decomposition of the compound. The DSC curves for **A1** and **A2** show sharp endothermic peaks at 196.0 and 211.0 °C which correspond to

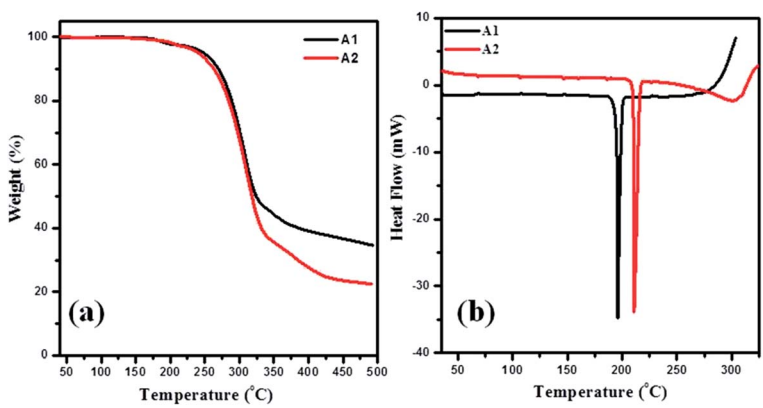

Fig. 8 (a) TGA and (b) DSC curves of **A1** and **A2**.

Table 3 Melting temperature, decomposition temperature, heat of fusion, entropy of fusion and thermal activation energy

Compound	T_m[a] (°C)	T_d[b] (°C)	ΔH_f[c] (kJ mol^{-1})	ΔS_f[d] (J K^{-1} mol^{-1})	Decomposition range (°C)	Corresponding E_a[e] (kJ mol^{-1})
A1	196	330	33.2	70.8	180–330	76.0
A2	211	335	39.9	82.6	200–335	104.0

[a] Melting temperature obtained from DSC. [b] Decomposition temperature obtained from DTA. [c] Heat of fusion calculated using DSC data. [d] Entropy of fusion calculated using DSC data. [e] Activation energy calculated using TGA data (details given in the ESI) in the particular decomposition region.

the melting temperature of **A1** and **A2**, respectively. The area under the peak represents the heat of fusion value of the compound. All the thermal data for **A1** and **A2** are summarized in Table 3.

4. Conclusions

We have discussed the role of molecular packing in the solid state light emitting properties of a simple benzene based D–π–A system containing methoxy group(s) as the electron donor and a cyano(aminocarbonyl)methylidene group as the electron acceptor. Both of the compounds possess strong fluorescence in the solid phase as compared with the solution phase, which is due to the existence of inter-fluorophore interactions in the solid phase. X-ray crystallographic studies revealed that the molecular packing of **A1** involves additional C–H$\cdots\pi$ interactions between the π-electron density of the benzene ring of one molecule and the vinyl hydrogen of another molecule. This C–H$\cdots\pi$ interaction strengthens the packing and causes greater RIR, resulting in AIEE in **A1**. High thermal stability (>300 °C) has been obtained for both compounds. Based on the present structure–property relationship study it can be concluded that in this particular D–π–A system, the solid state light emitting properties are sensitive to the nature and position of the donor groups. Further improvement of the properties might be possible in the future by modifying the skeleton of the π-conjugated spacer and by varying the functional groups.

Acknowledgements

V. K. Gupta gratefully acknowledges the University Grant Commission (UGC), New Delhi for the award of BSR meritorious fellowship.

References

1 C. Chen, X. H. Jin, X. J. Zhou, L. X. Cai, Y. J. Zhang and J. Zhang, Photo-facilitated aggregation and correlated color temperature adjustment of single component organic solid state white-light emitting material, *J. Mater. Chem. C*, 2015, **3**, 4563–4569.

2 J. Li, Y. Jiang, J. Cheng, Y. Zhang, H. Su, J. W. Y. Lam, H. H. Y. Sung, K. S. Wong, H. S. Kwok and B. Z. Tang, Tuning the singlet-triplet energy gap of AIE luminogens: crystallization-induced room temperature phosphorescence and delay fluorescence, tunable temperature response, highly efficient non-doped organic light-emitting diodes, *Phys. Chem. Chem. Phys.*, 2015, **17**, 1134–1141.

3 Q. Niu, Q. Zhang, W. Xu, Y. Jiang, R. Xia, D. D. C. Bradley, D. Li and X. Wen, Solution-processed anthracene-based molecular glasses as stable blue-light-emission laser gain media, *Org. Electron.*, 2015, **18**, 95–100.

4 B. Dong, M. Wang, C. Xu, Q. Feng and Y. Wang, Tuning solid-state fluorescence of a twisted π-conjugated molecule by regulating the arrangement of anthracene fluorophores, *Cryst. Growth Des.*, 2012, **12**, 5986–5993.

5 X. Y. Shen, W. Z. Yaun, Y. Liu, Q. Zhao, P. Lu, Y. Ma, I. D. Williams, A. Qin, J. Z. Sun and B. Z. Tang, Fumaronitrile-based fluorogen: red to near-infrared

fluorescence, aggregation-induced emission, solvatochromism, and twisted intramolecular charge transfer, *J. Phys. Chem. C*, 2012, **116**, 10541–10547.

6 J. Luo, Z. Xie, J. W. Y. Lam, L. Cheng, H. Chen, C. Qiu, H. S. Kwok, X. Zhan, Y. Liu, D. Zhu and B. Z. Tang, Aggregation-induced emission of 1-methyl-1,2,3,4,5-pentaphenylsilole, *Chem. Commun.*, 2001, 1740–1741.

7 B. Z. Tang, X. Zhan, G. Yu, P. P. S. Lee, Y. Liu and D. Zhu, Efficient blue emission from siloles, *J. Mater. Chem.*, 2001, **11**, 2974–2978.

8 Y. Hong, J. W. Y. Lam and B. Z. Tang, Aggregation-induced emission, *Chem. Soc. Rev.*, 2011, **40**, 5361–5388.

9 M. Shimada, Y. Yamanoi, T. Matsushita, T. Kondo, E. Nishibori, A. Hatakeyama, K. Sugimoto and H. Nishihara, Optical properties of disilane-bridged donor–acceptor architectures: strong effect of substituents on fluorescence and nonlinear optical properties, *J. Am. Chem. Soc.*, 2015, **137**, 1024–1027.

10 V. K. Gupta and R. A. Singh, An investigation on single crystal growth, structural, thermal and optical properties of a series of organic D–π–A push–pull materials, *RSC Adv.*, 2015, **5**, 38591–38600.

11 S. Son, H. Kim, H. Y. Yun, D. H. Kim, S. Ullah, S. J. Kim, Y. J. Kim, M. S. Kim, J. W. Yoo, P. Chun and H. R. Moon, (*E*)-2-Cyano-3-(substituted phenyl) acrylamide analogs as potent inhibitors of tyrosinase: A linear β-phenyl-α,β-unsaturated carbonyl scaffold, *Bioorg. Med. Chem.*, 2015, **23**, 7728–7734.

12 S. K. Rai, S. Khanam, R. S. Khanna and A. K. Tewari, Cascade synthesis of 2-pyridones using acrylamides and ketones, *RSC Adv.*, 2014, **4**, 44141–44145.

13 P. Hrdlovic, J. Donovalova, H. Stankovicova and A. Gaplovsky, Influence of polarity of solvents on the spectral properties of bichromophoric coumarins, *Molecules*, 2010, **15**, 8915–8932.

14 R. Davis, N. S. S. Kumar, S. Abraham, C. H. Suresh, N. P. Rath, N. Tamaoki and S. Das, Molecular Packing and Solid-State Fluorescenceof Alkoxy-Cyano Substituted Diphenylbutadienes: Structure of the Luminescent Aggregates, *J. Phys. Chem. C*, 2008, **112**, 2137–2146.

15 R. Davis, N. P. Rath and S. Das, Thermally reversible fluorescent polymorphs of alkoxy-cyano-substituted diphenylbutadienes: role of crystal packing in solid state fluorescence, *Chem. Commun.*, 2004, 74–75.

16 Q. Zeng, Z. Li, Y. Dong, C. Di, A. Qin, Y. Hong, L. Ji, Z. Zhu, C. K. W. Jim, G. Yu, Q. Li, Z. Li, Y. Liu, J. Qin and B. Z. Tang, Fluorescence enhancements of benzene-cored luminophors by restricted intramolecular rotations: AIE and AIEE effects, *Chem. Commun.*, 2007, 70–72.

17 J. Luo, Z. Xie, J. W. Y. Lam, L. Cheng, H. Chen, C. Qiu, H. S. Kwok, X. Zhan, Y. Liu, D. Zhuc and B. Z. Tang, Aggregation-induced emission of 1-methyl-1,2,3,4,5-pentaphenylsilole, *Chem. Commun.*, 2001, 1740–1741.

18 Y. Hong, J. Y. K. Lam and B. Z. Tang, Aggregation-induced emission, *Chem. Soc. Rev.*, 2011, **40**, 5361–5388.

19 N. Mataga, Y. Kaifu and M. Kolzumi, Solvent effects upon fluorescence spectra and the dipole moments of excited molecules, *Bull. Chem. Soc. Jpn.*, 1956, **29**, 465–470.

20 A. P. Demchenko, K. C. Tang and P. T. Chou, Excited-state proton coupled charge transfer modulated by molecular structure and media polarization, *Chem. Soc. Rev.*, 2013, **42**, 1379–1408.

21 S. Nad, M. Kumbhakar and H. Pal, Photophysical properties of coumarin-152 and coumarin-481 dyes: unusual behavior in nonpolar and in higher polarity solvents, *J. Phys. Chem. A*, 2003, **107**, 4808–4816.

22 Z. R. Grabowski and K. Rotkiewicz, Structural changes accompanying intramolecular electron transfer: focus on twisted intramolecular charge-transfer states and structures, *Chem. Rev.*, 2003, **103**, 3899–3931.

